Journal of Power Sources 196 (2011) 5342–5348

Contents lists available at ScienceDirect

Journal of Power Sources

journal homepage: www.elsevier.com/locate/jpowsour

Studies on $LiFePO_4$ as cathode material using impedance spectroscopy

Jan Philipp Schmidt*, Thorsten Chrobak, Moses Ender, Jörg Illig, Dino Klotz, Ellen Ivers-Tiffée

Institut für Werkstoffe der Elektrotechnik (IWE), Karlsruher Institut für Technologie, Adenauerring 20b, 76131 Karlsruhe, Germany

ARTICLE INFO

Article history:
Received 17 June 2010
Received in revised form
10 September 2010
Accepted 28 September 2010
Available online 2 December 2010

Keywords:
Lithium iron phosphate
Distribution of relaxation times (DRTs)
Electrochemical impedance spectroscopy (EIS)

ABSTRACT

Lithium iron phosphate is a promising cathode material for the use in hybrid electrical vehicles (HEV) meeting the demands of good stability during cycling and safe operation due to reduced risk of thermal runaway. However, slow solid state diffusion and poor electrical conductivity reduce power capability. For further improvement, the identification of the rate determining processes is necessary. Electrochemical impedance spectroscopy (EIS) has proven to be a powerful tool for the characterization of electrochemical systems. In this contribution a deconvolution of the impedance with the distribution of relaxation times (DRTs) is used to obtain a better resolution in frequency domain. Therewith, the relevant loss processes are identified and an impedance model is developed. Using DRT and CNLS-fit allows the determination of time constants and polarization resistances of all relevant loss processes. Furthermore, their temperature behavior is studied and a physical interpretation is provided.

1. Introduction

The automobile industry has established rigorous standards in terms of security and reliability. The success of electro mobility is strongly dependent on advances in lithium ion battery technology. In recent years, a spectrum of candidate materials for battery electrodes and electrolytes has been investigated. Since cathodes fall short of the theoretical capacity compared with typical anodes, many works concentrated on the knowledge and improvement of cathode materials [1–5].

After being proposed in 1997 as a potential candidate for the use in lithium ion batteries, lithium iron phosphate ($LiFePO_4$) has drawn much attention due to its good cycling behavior [1,4,6]. It offers a relatively large theoretical capacity of 170 mAh/g and allows a cell voltage of 3.4 V vs. Li, maximizing energy density while minimizing side reactions such as electrolyte decomposition [2,6]. Furthermore, analysis by differential scanning calorimetry (DSC) revealed excellent thermal stability in comparison with other established cathode materials like $LiCoO_2$ and $LiMn_2O_4$[7]. However, the positive aspects are counteracted by low electronic and ionic conductivities leading to a poor high power capability [2]. Rate performance as well as the charge and discharge capacity of $LiFePO_4$ is directly affected by the cell temperature. To improve the electrical and electrochemical properties of a $LiFePO_4$ cathode structure, the rate determining steps need to be clearly identified and thoroughly understood [4,8].

Along with cyclic voltammetry (CV), electrochemical impedance spectroscopy (EIS) has proven to be a powerful tool for characterization of electrochemical systems in general [1,8,9]. Impedance spectra, which contain information about the physico-chemical processes within the cell, are usually evaluated by an equivalent circuit model. This approach requires knowledge about number, and physical origin of all processes, that contribute to the cumulative impedance. Fig. 1 gives an qualitative overview of processes adding to ohmic, polarization as well as diffusion resistance in a cell with $LiFePO_4$ cathode structure and the order of magnitude of their expected frequency range as given in [10,11]. Processes, which can be assigned to the lithium metal counter electrode, are not considered in this figure. As these processes lower the voltage of the cell by causing an overvoltage during operation, these processes will be further considered as loss processes. The identification even of the most prominent loss processes and the determination of their specific time constants remain ambiguous, as they usually overlap. This challenge can be addressed by a deconvolution of the impedance with the distribution of relaxation times (DRTs). This advanced method has been developed for and successfully applied in high temperature fuel cell research, where a physically motivated impedance model without the need of any a priori knowledge of the investigated electrochemical system was generated. The DRT method offers a higher resolution in the frequency domain, allowing a clearer identification of the loss processes [12–14].

In the present work, three cell configurations, (a) full cells ($LiFePO_4$/Li), (b) symmetrical cathode cells ($LiFePO_4$/$LiFePO_4$) and (c) symmetrical anode cells (Li/Li) are evaluated. The symmetrical setup allows to separate anodic and cathodic loss processes. All

* Corresponding author. Tel.: +49 721 6087583; fax: +49 721 6087492.
E-mail address: jan.schmidt@kit.edu (J.P. Schmidt).

0378-7753/$ – see front matter © 2010 Elsevier B.V. All rights reserved.
doi:10.1016/j.jpowsour.2010.09.121

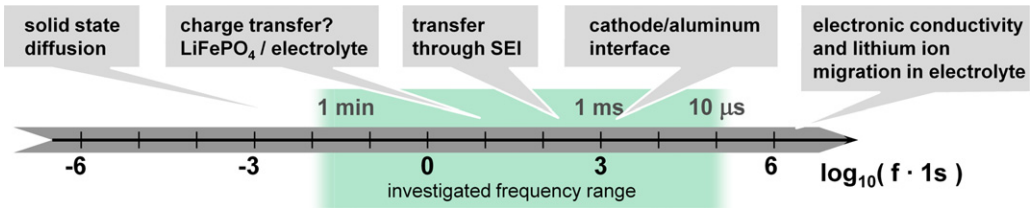

Fig. 1. Most prominent loss processes in a lithium ion cell with a $LiFePO_4$ cathode structure, sorted by their potential characteristic frequencies.

test cells are analyzed by impedance spectroscopy in a temperature range of 0–40 °C. The low frequency branch of the EIS-spectra is modeled by a series of a capacity C and a generalized finite length Warburg (GFLW) and then subtracted. For the remaining impedance data the distribution of relaxation times (DRTs) is calculated. This two-step pre-identification of all relevant loss processes and their time constants, leads to an equivalent circuit model, which is finally used to derive the area specific resistance (ASR) and activation energy (E_a) for all processes found. This methodology constitutes a new approach to investigate lithium ion battery electrodes, delivering an accurate separation of two loss processes in the $LiFePO_4$ cathode.

2. Experimental

For this study, cathodes were prepared from basic carbon coated $LiFePO_4$ powder (Sued-Chemie AG), to which carbon black and PVDF-binder were added to receive a final weight ratio of 70:24:6 ($LiFePO_4$:carbon black:binder). The mass of active material in each cathode was about 1.5 mg. Thereafter, a 1-methyl-2-pyrrolidinone (NMP) based slurry was prepared, applied on an aluminum foil by doctor-coating and vacuum dried for 120 min at 80 °C. The electrodes were punched out and finally tempered for another 180 min at 120 °C.

All measurements were conducted on Swagelok-type test cells in three different configurations: full cells with $LiFePO_4$ vs. metallic lithium (a), as well as symmetrical setups with $LiFePO_4$ vs. $LiFePO_4$ (b) and lithium vs. lithium (c). All investigated cells featured electrodes with 1.2 cm in diameter and an active area of 1.13 cm^2 respectively. The metallic lithium foil (Sigma–Aldrich) had a thickness of 0.38 mm which resulted in a mass of active material around 23.3 mg. This guaranteed a sufficiently high lithium reservoir for the examination of cathode material. The separators of all cells consisted of two layers, a Freudenberg FS2019 serving as an electrolyte reservoir and a Celgard C500 membrane, to prevent short-circuiting. The electrolyte used was a 1 mol lithium perchlorate ($LiClO_4$) solution, based on ethylene carbonate (EC) and ethyl methyl carbonate (EMC) with a gravimetric mixing ratio of 1:1.

After cell assembly, ten charge and discharge cycles were performed to ensure a steady state of the system (compare Fig. 3). Impedance measurements were carried out using the Solartron 1400E cell test system with Scribner Multistat software. The applied ac voltage was 10 mV (RMS) at open circuit condition and the frequency was varied within a range of 1 MHz–10 mHz. The quality of the obtained impedance data was analyzed by calculating the Kramers–Kronig residuals. Within the frequency range from 10 mHz up to 100 kHz, the residuals (real and imaginary parts) were below 0.5%, proving high data quality of all conducted impedance measurements. Therefore only the frequency range from 100 kHz to 10 mHz was used for further analysis. All impedance spectra were measured at a state of charge of 100% for the cell system, which means a fully deintercalated state for the $LiFePO_4$, varying temperature between 0 ° C and 40 ° C in a climate test chamber. At least four identical cells have been measured in parallel to validate the reproducibility of the results.

3. DRT and preprocessing

The distribution of relaxation times (DRTs) is a recommendable method to deconvolute impedance data, because of its outstanding potential to resolve polarization processes with close-up time constants [12–14]. Contrary to a fit procedure with equivalent circuits, the individual processes that contribute to the overall impedance are represented without any assumption for their physical origins. Although the DRT has proven to be a useful tool for the investigation of high temperature fuel cells [12–14] and has been examined by other researchers [15–17] it remained widely unknown – probably because of its high portion of signal processing. The relation between the impedance and its DRT is given by

$$Z(\omega) = R_0 + Z_{pol}(\omega) = R_0 + R_{pol}\int_0^\infty \frac{g(\tau)}{1+j\omega\tau}\mathrm{d}\tau \quad (1)$$

with the condition that

$$\int_0^\infty g(\tau)\,\mathrm{d}\tau = 1 \quad (2)$$

where $Z(\omega)$ is the impedance data, R_0 is the ohmic part of the impedance, $Z_{pol}(\omega)$ is the polarization part, R_{pol} is the polarization resistance of the impedance and $g(\tau)$ is the corresponding distribution of relaxation times. The expression in the integral resembles the definition of an RC-element:

$$Z_{RC}(\omega) = \frac{R}{1+j\omega\tau} = \frac{R}{1+j\omega RC} \quad (3)$$

If the distribution of relaxation times $g(\tau)$ is a sum of Dirac-pulses

$$g(\tau) = \sum_{n-1}^{N}\delta(\tau-\tau_n) \quad (4)$$

the integral represents a series connection of N RC-elements with individual relaxation time constants τ_i. Fig. 2a demonstrates the advantage of the DRT for the simple case of $N = 2$. In the Nyquist plot the two RC-arcs hardly can be distinguished while its representation in the DRT clearly shows two Dirac impulses corresponding to two RC-elements. The height of the peak equals the polarization R and its position sets the relaxation time τ_i or characteristic frequency.

RC-elements describe an “ideal” system with lumped parameters whereas RQ-elements are an adequate representation for “real” electrochemical systems with distributed parameters. The RQ-element is here defined as:

$$Z_{RQ}(\omega) = \frac{R}{1+(j\omega RQ)^\eta} \quad (5)$$

Fig. 2b shows the DRT of 2 RQ-elements with a broadened distribution curve and two maxima on mean value of the distribution of relaxation times. The integral over a single peak represents the polarization R in the definition of the RQ-element, its center the relaxation time

$$\tau = \frac{1}{RQ} \quad (6)$$

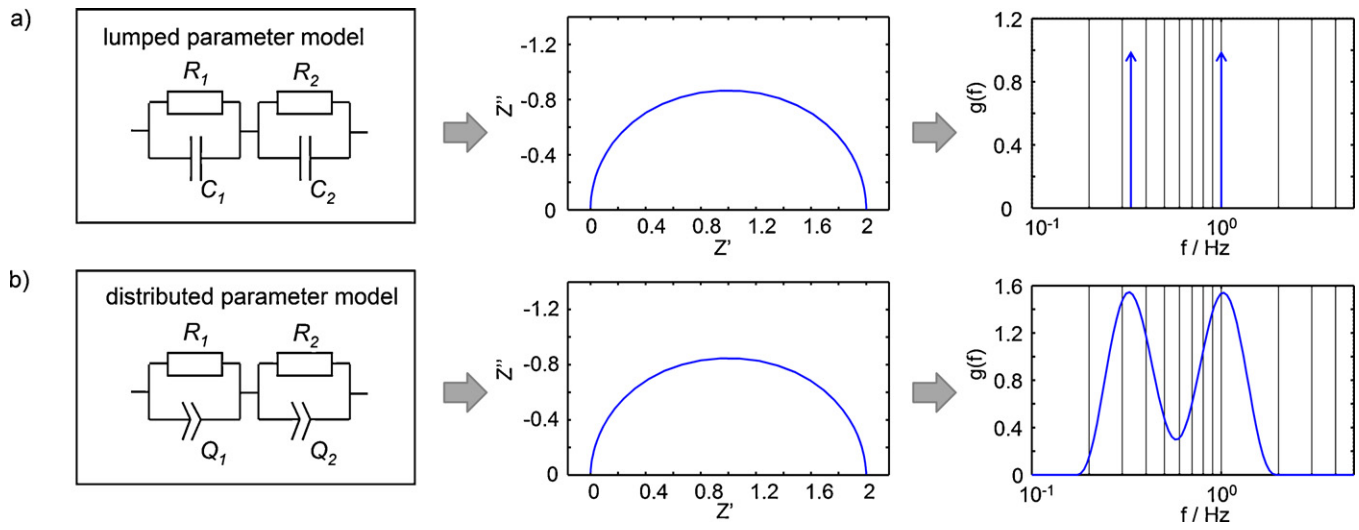

Fig. 2. Nyquist plot (center) and distribution function of relaxation times (right) for two different systems: (a) lumped parameter model with two series RC-elements, (b) distributed parameter model with two series RQ-elements.

The DRT representation of the 2 RQ-elements gives a clear proof for its superiority, as both processes are separated and their characteristic frequencies are apparent. For the first time, the DRT shall now proof its usefulness to the separation of electrochemical loss processes in lithium ion cells. However, in contrast to high temperature fuel cells, an extension of the DRT-method is essential for the investigation of lithium ion cells.

The distribution of relaxation times $g(\tau)$ in Eq. (1) is expressed as an integral from zero to infinity. Furthermore, impedance measurements of lithium ion cells never cover the entire frequency range. This problem dissolves if all processes lie inside the measured frequency range. However, the low frequency processes in the mHz-range (e.g. solid state diffusion) are (at least partly) excluded due to the long measurement time.

Another difficulty is that the impedance spectra of lithium ion cells always include a series capacity or a differential intercalation capacity, as explained in [10]. As the distribution of relaxation times $g(\tau)$ in Eq. 1 does not include pure capacitive behavior, it is mandatory to eliminate the series capacity in a preprocessing step.

The differential intercalation capacity and the solid state diffusion are divided from the entire impedance expression by the following procedure, consisting of three consecutive steps:

1. Modeling the low frequency branch (preprocessing).
2. Subtraction of the low frequency branch (preprocessing).
3. Evaluation of the resulting spectra by DRT-approach (main step).

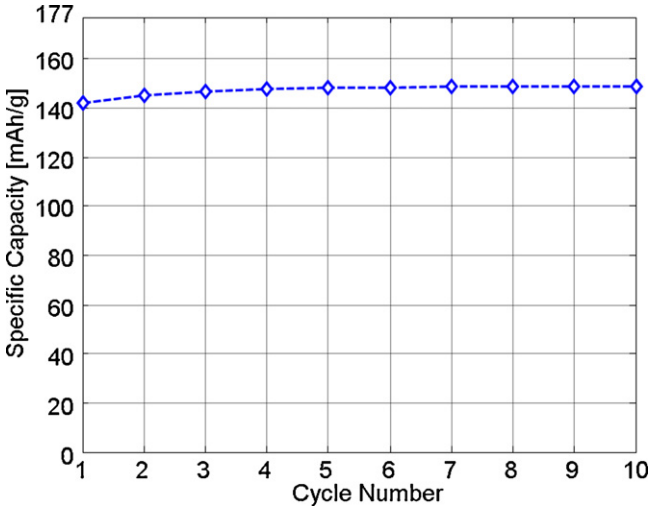

Fig. 3. Specific discharge capacity of one $LiFePO_4$ cell during the formation, corresponding to its mass of active material. The capacity is very stable which indicates a steady state.

As a prerequisite, the low frequency branch must be physically reasonable modeled, fitted and subtracted. In agreement with literature, we assigned the low frequency branch to (i) solid state diffusion in the intercalation electrode and (ii) to intercalation capacity [10,18,19]. Modeling approaches are described in [10,20], we made use of the diffusion and intercalation model proposed by Levi and Aurbach [10] comprising of a finite length Warburg element and a series capacity. This model approach was also justified by the theoretical work of Jacobsen and West [21] for diffusion in a spherical particle with diffusion towards the center. Herein the behaviour at high frequencies is equivalent to a finite length Warburg impedance in series with a capacity. This modeling approach leads to the impedance

$$Z_{Diff} = Z_W + Z_C = R_W \cdot \frac{\tanh\left([j\tau_W\omega]^{P_W}\right)}{[j\tau_W\omega]^{P_W}} + \frac{1}{j\omega C_0} \tag{7}$$

Fig. 4a shows step 1 of the preprocessing: the resulting CNLS fit of this model to the measured impedance curve. Accordingly, Fig. 4b shows step 2 of the preprocessing: it is now subtracted from the measurement data and brings out an impedance that can be deconvoluted. Implicitly, two equations have been applied:

1. The (total) impedance is assumed as one part that can be described by the DRT and another part resulting from solid state diffusion/intercalation and cell capacity

$$Z_{tot}(j\omega) = R^*_{pol}\int_0^\infty \frac{g(\tau)}{1+j\omega\tau}\mathrm{d}\tau + Z_{FLW} + Z_C \tag{8}$$

2. Solid state diffusion/intercalation capacity is subtracted from the measured (total) impedance

$$Z_{pre}(j\omega) \quad = Z_{tot} - Z_{FLW} - Z_C = R^*_{pol}\int_0^\infty \frac{g(\tau)}{1+j\omega\tau}\mathrm{d}\tau \tag{9}$$

4. Results and discussion

Fig. 5a shows on the left hand side the preprocessed impedance curves of $LiFePO_4$/Li-cells for varying temperatures between 0 °C

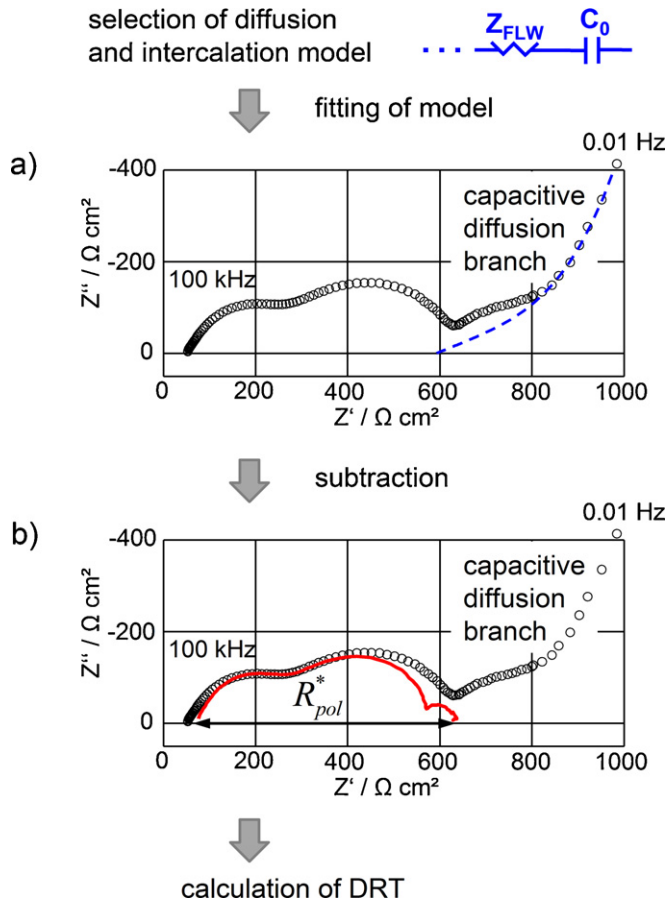

Fig. 4. Different stages of preprocessing of impedance data: (a) fitting of diffusion and intercalation model to the impedance data and subsequent subtraction; (b) preprocessed impedance to be evaluated by the DRT.

and 40 °C. The impedance curves reveal an increasing overall polarization and ohmic resistance for decreasing temperatures. Furthermore, they show an increasing number of polarization processes. For the 0 ° C measurement, three polarization processes can be identified. Fig. 5a shows on the right the corresponding DRT of these impedance curves. Even for 40 ° C it is possible to separate five polarization processes by the DRT, whereas the impedance curve only reveals two distinctive processes.

Over the entire temperature range, there are three major loss processes which are examined in the following study. The DRT illustrates that process P_{1C} has an increasing polarization and a decreasing characteristic frequency (10–0.2 Hz) for decreasing temperatures. This behavior is also shown for process P_{1A}, whereas this process plays a major role in the overall polarization. Process P_{2C} at 1 kHz represents the main loss process for most temperatures and is almost temperature independent. The two small high frequency processes cause a minor part of the overall cell impedance and their frequencies overlap for low temperatures. For a consistent evaluation of these two processes, a detailed examination in further studies is required. In this first approach they are neglected.

For an assignment of these three major loss processes to cathode and anode sides, symmetrical test cells were assembled. The impedance measurements of the symmetrical $LiFePO_4$ cell are shown in Fig. 5b. The temperature variation exhibits two major loss processes. The DRT in Fig. 5b on the right hand side deconvolutes very clearly these two loss processes and their temperature dependency. The low frequency process contributes the minor part to the polarization of the cathode and shows a strongly varying characteristic frequency (0.2–2 Hz). The other process has a relaxation frequency around 2 kHz and is almost temperature independent.

The impedance curves for the symmetrical Li/Li-cells are shown in Fig. 5c on the left hand side. The polarization of the impedance curve is increasing significantly with decreasing temperature and one major loss process can be identified. The corresponding DRT in figure Fig. 5c on the right shows that the characteristic frequency of this process is shifting from 800 Hz down to 100 Hz. Furthermore,

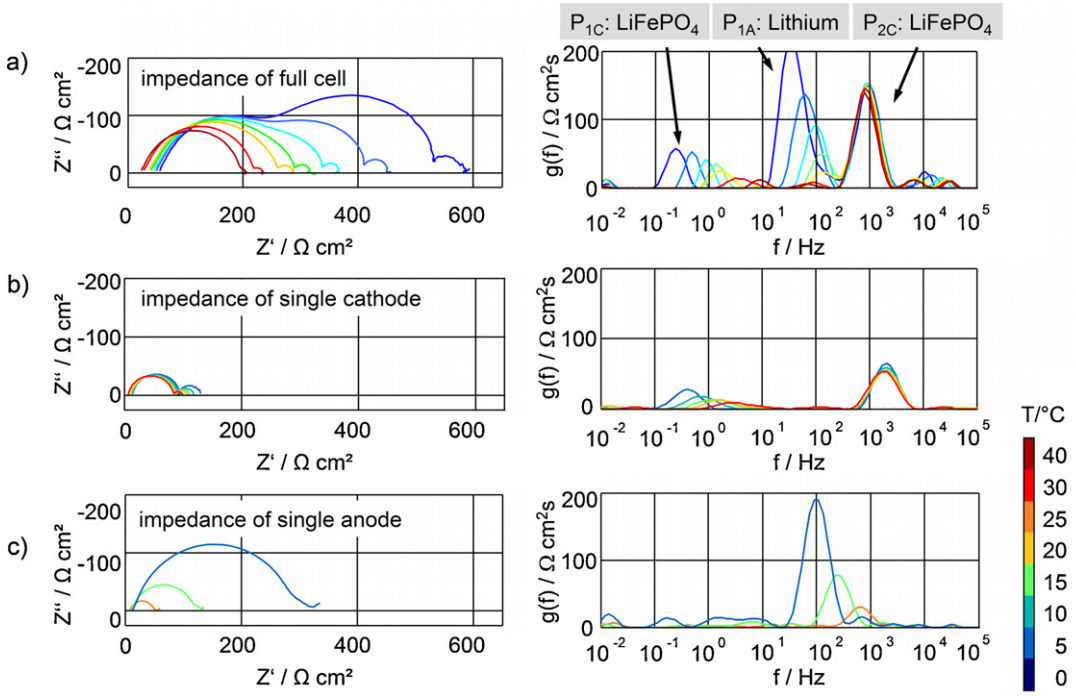

Fig. 5. Pre-processed impedance curves (left column) for the three investigated cell configurations: (a) $LiFePO_4$/Li-cells, (b) symmetrical $LiFePO_4$/$LiFePO_4$-cells and (c) symmetrical lithium/lithium-cells and their corresponding distributions of relaxation times (right column).

for low frequencies, the DRT shows an indefinite number of loss processes. In the impedance curve this is represented by the flat low frequency part of the semi circle. This low frequency domain must be examined in detail to understand the Li-anode behavior. However, in this study, the Li/Li-cell is used for the separation of anodic and cathodic loss processes which is done in the following section.

4.1. Identification of loss processes and assignment to the electrodes

For this purpose, symmetrical cells and $LiFePO_4$/Li-cells are compared in Fig. 5. On the left hand side, the impedance curves are aligned vertically. The symmetrical cells show different polarization amplitudes than the half cell impedance curves and do not allow an assignment of cathode or anode processes. The right column of Fig. 5 shows the DRTs of all measurements and illustrates one main advantage of the DRT visualization. Processes one and three are directly re-detected in the symmetrical cathode cell by comparing their characteristic frequency and their temperature behavior. Similarly, process two is re-detected in the symmetrical anode cell. An assignment of these major loss processes of the $LiFePO_4$/Li-cell to anode and cathode by DRT is possible. In the following sections, processes one, two and three are therefore called P_{1C}, P_{1A} and P_{2C}.

The exploitation of the DRT's advantages and symmetrical cell measurements enables a clear assignment of cathode and anode processes. However, as mentioned before, the same processes in different cell configuration have slightly different characteristic frequencies and show a little different temperature behavior. This might be a hint on difficulties of homogeneous composite layer fabrication or different aging statuses of the measured cells. Nevertheless, this shows the manifold prospects of the impedance analysis by using the DRT approach.

4.2. Equivalent circuit model

The preidentification of all relevant loss processes and the determination of their electrode origin lead to an equivalent circuit model which can be seen in Fig. 6. It consists of the predetermined finite length Warburg element with a serial capacity, representing the solid state diffusion and the differential capacity of the cell [10]. Furthermore, there are three RQ-elements, representing the major loss processes P_{1A}, P_{1C} and P_{2C}, which were identified by the DRT approach. As the other small processes P_4 and P_5 only cause a minor part of the overall cell impedance, they are neglected in this first approach. Lastly, the model contains a serial resistance for the limited electronic and ionic conductivities of all cell components and an inductor for modeling the cable inductivity. For frequencies up to 100 kHz, this is not relevant for the measured test cells. In the following, this model is used for analyzing the temperature behavior of the relevant loss processes by CNLS-fit in Matlab®. The applied starting values for the fitting procedure were directly obtained from the DRT. The model was fitted to impedance curves for different temperatures and the fit results were evaluated. Table 1 contains a listing of the temperature specific characteristics of each process. Column two shows the characteristic frequencies obtained from DRT while column three contains the area specific resistances (ASRs) obtained from model fit. For further analysis of the obtained model fit and a detailed examination of each process, the activation energies are calculated in the next section.

Table 1
Characteristic frequency and area specific resistance (ASR) of all identified processes at 0 and 40 °C.

Process	f_r (Hz)	ASR (Ω cm²)	T (°C)
R_0	–	52	0
		17	40
P_{1A}	30	239	0
	200	19	40
$P_{diff,C}$	0.001	1037	0
	0.02	110	40
P_{1C}	0.3	50	0
	10	7	40
P_{2C}	1000	213	0
	1000	137	40

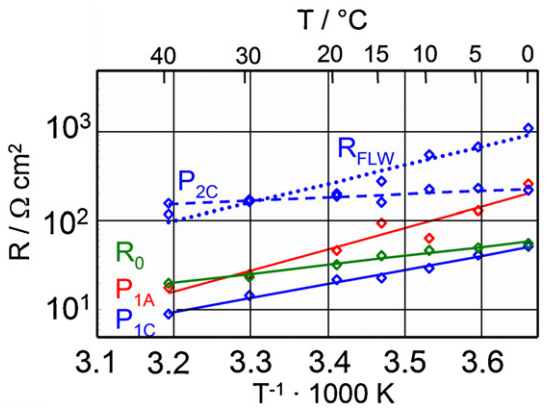

Fig. 7. Arrhenius behavior of all observed processes, indicating a reasonable fit result over the entire temperature range from 0 to 40 °C.

4.3. Activation energies

There are several reasons for calculating the activation energies of electrochemical processes. The first one is checking if the obtained fit parameter exhibits Arrhenius type behavior which indicates a reasonable fit result. Fig. 7 provides the Arrhenius plots of all polarization processes. The resistance values follow nicely to Arrhenius behavior which shows that the model fit for varying tem-

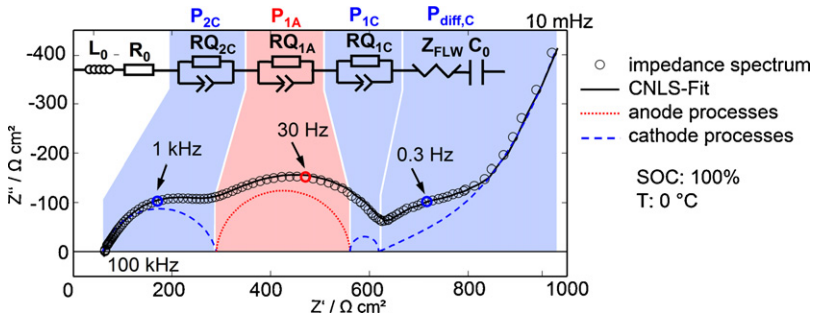

Fig. 6. Equivalent circuit model derived from combined analysis of impedance spectra and symmetrical cell configurations by using the DRT method.

Table 2
Comparison of the determined activation energies and area specific resistances (ASRs) at 25 ◦ C of all loss processes and reported literature values. Physical origins of all loss processes are given in the right column.

Process	ASR (25 °C) (Ω cm^2)	E_{act} (eV)	$E_{act,lit}$ (eV)	Literature	Physical origin
R_0	28	0.20	0.18–0.3	Dasgupta et al. [22]	Electronic conductivity (carbon black)
			0.017	Chagnes et al. [23]	Ionic conductivity ($LiClO_4$)
P_{1A}	37.4	0.47	0.49–0.83	Zaban et al. [24]	Charge transfer Li/SEI
$P_{diff,C}$	207.6	0.66	0.4–0.95	Takahashi et al. [7]	Solid state diffusion in $LiFePO_4$
				Maier and Amin [25]	
P_{1C}	16.5	0.31	–	–	Charge transfer between electrolyte and $LiFePO_4$
P_{2C}	176	0.07	–	Gaberscek et al. [8]	Cathode/aluminum interface

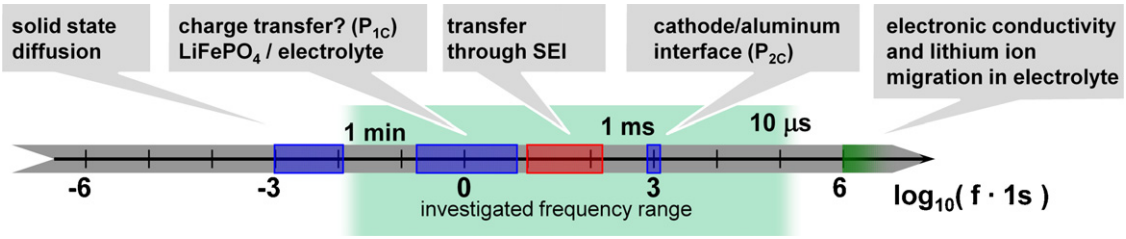

Fig. 8. Observed frequency ranges of the identified loss processes in our $LiFePO_4$/Li-cells.

peratures works consistently. Table 2 lists the calculated values for activation energies.

The next step for exploiting the information content of activation energies is the comparison with literature values. In this way, the reasonability of the determined values and the physical origin of the respective process can be examined. Table 2 compares the calculated activation energies for each process to reported literature values.

The ohmic resistance has several physical reasons. Generally, it is caused by the limited electronic and ionic conductivities of all cell components. Comparing the activation energy of the ohmic resistance to the activation energy of carbon black conductivity and $LiClO_4$-conductivity (see Table 2) gives further information. The value of 0.2 eV lies in the range of activation energies of amorphous carbon conductivity [22]. This suggests that the major part of the ohmic losses in our cathode is caused by this low conductivity of the cathode composite. However one has to keep in mind, that this strongly depends on the used materials and the preparation process and might be completely different for other $LiFePO_4$ cells.

The anode loss process activation energy being 0.47 eV is very close to the values reported by Zaban et al. [24], which are charted in Table 2. According to [24,26], P_{1A} is mainly caused by lithium migration through several SEI layers.

For the $LiFePO_4$-cathode, there are three relevant polarization processes detected. The first process $P_{diff,C}$ was pre-determined to be the solid state diffusion. In order to obtain the activation energy of solid state diffusion, diffusion coefficients were determined and fitted by an Arrhenius equation. A value of 0.66 eV was obtained for activation energy which is between the reported literature values (see Table 2).

There are two further cathode loss processes which must be examined. The activation energy for P_{1C} in the low frequency region was determined to be 0.31 eV while for P_{2C} the value of 0.07 eV was obtained. In literature, a value of 0.15 eV was reported by Takahashi et al. [7] for the high frequency loss process which corresponds to P_{2C} in this study. However, Takahashi et al. did not observe a second loss process which indicates that P_{1C} and P_{2C} overlapped in his evaluation.

The identification of two cathode loss processes was reported in [8] by Gaberscek et al. Gaberscek determined P_{2C} to be the interface between electrode composite and aluminum current collector whereas for P_{1C}, no physical interpretation is provided. The low activation energy being 0.07 eV in this study supports this physical interpretation for P_{2C}.

A possible interpretation for P_{1C} regarding the higher activation energy is the charge transfer between electrolyte and cathode composite. Further investigations are necessary to confirm this assumption. A line up of all determined loss processes according to their characteristic frequency is given in Fig. 8.

5. Conclusions

Lithium iron phosphate ($LiFePO_4$) has drawn much attention as cathode material, but low electronic and ionic conductivities lead to a poor high power capability. Moreover, the rate determining steps need to be clearly identified and thoroughly understood.

Electrochemical impedance spectroscopy was conducted on Swagelok-type test cells in three different configurations: full cells with $LiFePO_4$ vs. metallic lithium, symmetrical setups with $LiFePO_4$ vs. $LiFePO_4$ and lithium vs. lithium. For the first time, the evaluation of impedance data was successfully supported by the DRTs (distribution of relaxation times) method. This approach included a preprocessing by modeling the low frequency branch (<0.1 Hz) by a series connection of capacity (C) and generalized finite length Warburg (GFLW).

For the full cell with $LiFePO_4$, we propose an equivalent circuit model with 5 elements in series, namely (i) an ohmic resistance for electrolyte conductivity and electronic losses, three RQ-elements which represent the fast cathode process P_{2C} (cathode/aluminum interface according to [8]) (ii), the charge transfer process at the anode P_{1A} (iii) and the slower cathode process P_{1C} (charge transfer, to be confirmed by further experiments) (iv). The low frequency branch $P_{diff,C}$ is modeled by a combination of a finite length Warburg and a capacity (v). This model was capable of analyzing the area specific resitstance (ASR) and activation energy (E_{act}) separately for electrolyte, anode and cathode by CNLS-fit in Matlab®.

Three major loss processes of our $LiFePO_4$ cathode structures were attributed to physical processes according to the indication attained from the comparison of the resulting activation energies with literature data:

- Solid state diffusion/intercalation: ASR (25 °C) = 207.6 Ω cm^2, E_{act} = 0.66 eV.

- Charge transfer at the cathode/aluminum interface: ASR (25 °C) = 176 Ω cm^2, E_{act} = 0.07 eV.
- P_{1C} (probably the charge transfer at the cathode/electrolyte interface): ASR (25 °C) = 16.5 Ω cm^2, E_{act} = 0.31 eV

Acknowledgements

The authors gratefully acknowledge the collaboration with ISC-Würzburg from where the cathode material was delivered. Special thanks to Henning Lorrmann for the good collaboration. Furthermore, we appreciate the support of our colleagues Dr. -Ing. André Leonide and Dr. -Ing. André Weber.

This research and development project is funded by the Federal Ministry of Education and Research within the Framework Concept KoLiWIn (fund number 03SF0343H) and managed by the Project Management Agency Forschungszentrum Jülich (PTJ). All responsibilities for this publication rest with the authors.

References

[1] A. Padhi, K. Nanjundaswamy, J. Goodenough, Phospho-olivines as positive-electrode materials for rechargeable lithium batteries, Journal of the Electrochemical Society 144 (4) (1997) 1188–1194.
[2] V. Srinivasan, J. Newman, Discharge model for the lithium iron-phosphate electrode, Journal of the Electrochemical Society 151 (10) (2004) A1517–A1529, doi:10.1149/1.1785012.
[3] M.A. Roscher, J. Vetter, D.U. Sauer, Characterisation of charge and discharge behaviour of lithium ion batteries with olivine based cathode active material, Journal of Power Sources 191 (2) (2009) 582–590, doi:10.1016/j.jpowsour.2009.02.024.
[4] M. Winter, J. Besenhard, M. Spahr, P. Novak, Insertion electrode materials for rechargeable lithium batteries, Advanced Materials 10 (10) (1998) 725–763.
[5] J. Tarascon, M. Armand, Issues and challenges facing rechargeable lithium batteries, Nature 414 (6861) (2001) 359–367.
[6] D.D. MacNeil, Z. Lu, Z. Chen, J.R. Dahn, A comparison of the electrode/electrolyte reaction at elevated temperatures for various Li-ion battery cathodes, Journal of Power Sources 108 (1–2) (2002) 8–14, doi:10.1016/S0378-7753(01)01013-8.
[7] M. Takahashi, S. Ichi Tobishima, K. Takei, Y. Sakurai, Reaction behavior of $LiFePO_4$ as a cathode material for rechargeable lithium batteries, Solid State Ionics 148 (3–4) (2002) 283–289, doi:10.1016/S0167-2738(02)00064-4.
[8] M. Gaberscek, J. Moskon, B. Erjavec, R. Dominko, J. Jamnik, The importance of interphase contacts in Li ion electrodes: the meaning of the high-frequency impedance arc, Electrochemical and Solid-State Letters 11 (10) (2008) A170–A174, doi:10.1149/1.2964220.
[9] J.R.H. Macdonald (Ed.), Impedance Spectroscopy: Emphasizing Solid Materials and Systems, A Wiley-Interscience Publication, Wiley, New York, NY, 1987.
[10] M. Levi, D. Aurbach, Simultaneous measurements and modeling of the electrochemical impedance and the cyclic voltammetric characteristics of graphite electrodes doped with lithium, Journal of Physical Chemistry B 101 (23) (1997) 4630–4640.
[11] A. Jossen, Fundamentals of battery dynamics, Journal of Power Sources 154 (2) (2006) 530–538, selected papers from the Ninth Ulm Electrochemical Days. doi:10.1016/j.jpowsour.2005.10.041. http://www.sciencedirect.com/science/article/B6TH1–4HP6G8C-3/2/3f7544a06aa39abad3c51eee6e76f7cb.
[12] H. Schichlein, A. Müller, M. Voigts, A. Krügel, E. Ivers-Tiffée, Deconvolution of electrochemical impedance spectra for the identification of electrode reaction mechanisms in solid oxide fuel cells, Journal of Applied Electrochemistry 32 (8) (2002) 875–882, doi:10.1023/A:1020599525160.
[13] A. Leonide, V. Sonn, A. Weber, E. Ivers-Tiffée, Evaluation and modeling of the cell resistance in anode-supported solid oxide fuel cells, Journal of the Electrochemical Society 155 (1) (2008) B36–B41, doi:10.1149/1.2801372.
[14] V. Sonn, A. Leonide, E. Ivers-Tiffée, Combined deconvolution and CNLS fitting approach applied on the impedance response of technical ni/8ysz cermet electrodes, Journal of The Electrochemical Society 155 (7) (2008) B675–B679, doi:10.1149/1.2908860.
[15] J.R. Macdonald, E. Tuncer, Deconvolution of immittance data: some old and new methods, Journal of Electroanalytical Chemistry 602 (2) (2007) 255–262, doi:10.1016/j.jelechem.2007.01.006.
[16] E. Tuncer, J. R. MacDonald, Comparison of methods for estimating continuous distributions of relaxation times, Journal of Applied Physics 99 (7) (2006) 074106-+. arXiv:arXiv:cond-mat/0504428, doi:10.1063/1.2188053.
[17] B.A. Boukamp, J.R. Macdonald, Alternatives to Kronig–Kramers transformation and testing, and estimation of distributions, Solid State Ionics 74 (1–2) (1994) 85–101, doi:10.1016/0167-2738(94)90440-5.
[18] M. Levi, G. Salitra, B. Markovsky, H. Teller, D. Aurbach, U. Heider, L. Heider, Solid-state electrochemical kinetics of Li-ion intercalation into $Li_{1-x}CoO_2$: simultaneous application of electroanalytical techniques SSCV, PITT, and EIS, Journal of the Electrochemical Society 146 (4) (1999) 1279–1289.
[19] M. Doyle, J.P. Meyers, J. Newman, Computer simulations of the impedance response of lithium rechargeable batteries, Journal of the Electrochemical Society 147 (1) (2000) 99–110, doi:10.1149/1.1393162.
[20] M.D. Levi, C. Wang, D. Aurbach, Two parallel diffusion paths model for interpretation of pitt and eis responses from non-uniform intercalation electrodes, Journal of Electroanalytical Chemistry 561 (2004) 1–11, doi:10.1016/j.jelechem.2003.07.014.
[21] T. Jacobsen, K. West, Diffusion impedance in planar, cylindrical and spherical symmetry, Electrochimica Acta 40 (2) (1995) 255–262, doi:10.1016/0013-4686(94)E0192-3.
[22] D. Dasgupta, F. Demichelis, A. Tagliaferro, Electrical conductivity of amorphous carbon and amorphous hydrogenated carbon, Philosophical Magazine Part B 63 (3) (1991) 1255–1266, doi:10.1080/13642819108205558.
[23] A. Chagnes, B. Carr, P. Willmann, D. Lemordant, Ion transport theory of nonaqueous electrolytes. $LiClO_4$ in [gamma]-butyrolactone: the quasi lattice approach, Electrochimica Acta 46 (12) (2001) 1783–1791, doi:10.1016/S0013-4686(00)00718-0.
[24] A. Zaban, E. Zinigrad, D. Aurbach, Impedance spectroscopy of Li electrodes. 4. A general simple model of the Li-solution interphase in polar aprotic systems, Journal of Physical Chemistry 100 (8) (1996) 3089–3101.
[25] J. Maier, R. Amin, Defect chemistry of $LiFePO_4$, Journal of the Electrochemical Society 155 (4) (2008) A339–A344, doi:10.1149/1.2839626.
[26] D. Aurbach, A. Zaban, Impedance spectroscopy of lithium electrodes. Part 1. General behavior in propylene carbonate solutions and the correlation to surface chemistry and cycling efficiency, Journal of Electroanalytical Chemistry 348 (1–2) (1993) 155–179, an International Journal Devoted to all Aspects of Electrode Kinetics, Interfacial Structure, Properties of Electrolytes, Colloid and Biological Electrochemistry. doi:10.1016/0022-0728(93)80129-6.